River Flow 2020 – Uijttewaal et al (eds)
© 2020 Taylor & Francis Group, London, ISBN 978-0-367-62773-7

Porous shallow water modelling in differential form: Computation of cell-based conveyance porosity fields in a real urban layout

D.P. Viero & A. Defina
Department of Civil, Environmental and Architectural Engineering, University of Padova, Padova, Italy

A. Ferrari, R. Vacondio & P. Mignosa
Department of Engineering and Architecture, University of Parma, Parma, Italy

ABSTRACT: In the framework of porosity models for urban floods, this work presents a method to compute the spatial distribution of the porosity parameters for a real urban district. Specifically, the method estimates the four parameters required by the differential, dual-porosity formulation, in which an isotropic porosity accounts for the reduced storage volume due to buildings, and cell-based conveyance porosities are introduced in the momentum equations in tensor form to model anisotropic resistances and alterations in the flow direction. The algorithm evaluates the porosity parameters on a cell-by-cell basis and only resorting to geometrical information. The proposed method is tested by simulating the flooding of a real, complex urban district in Italy.

1 INTRODUCTION

In the framework of urban flood modelling, the 2D Shallow Water Equations (2D-SWEs) with porosity allow accounting for the presence of buildings and obstacles without resolving their geometry explicitly; the use of coarse meshes reduces run times and computational needs up to two orders of magnitude (if compared with high-resolution grids).

Several schemes of artificial porosity models were developed in the years, following either a differential approach (Defina 2000, Guinot & Soares-Frazão 2006, Cea & Vázquez-Cendón 2010, Finaud-Guyot et al. 2010, Velickovic et al. 2017, Ferrari et al. 2017, Cozzolino et al. 2018) or an integral approach (Sanders et al. 2008, Özgen et al. 2016, Bruwier et al. 2017, Guinot et al. 2017). The differential approach was originally developed based on the concept of Representative Elementary Area, whose size is significantly greater than the typical size of buildings (Guinot 2012). The integral approach was specifically developed to resolve the flow field at finer spatial scales (Sanders et al. 2008), yet being strongly dependent on the mesh design. Recently, Varra et al. (2019) showed that resorting to the differential approach does not prevent a model to supply meaningful information at the scale comparable to those of buildings (meters or tens of meters).

We recently proposed a dual-porosity model in differential form, (Ferrari et al. 2019, Viero 2019), in which an isotropic porosity accounts for the reduced storage volume due to buildings and a directionally-dependent conveyance porosity is introduced in the momentum equations in tensor form to model anisotropic resistances (Ferrari et al. 2019) and accelerations as well (Viero 2019), thus allowing capturing alterations in the flow direction due to buildings and obstacles. In these works, the model was tested on idealized and relatively small urban patches by evaluating the porosity parameters according to simple criteria and assuming them uniform within the urban area. It was shown that the anisotropic dual-porosity model is able to estimate well the directionally-dependent, overall resistance exerted by a patch of urbanized areas on the surrounding flow.

However, it must be pointed out that the use of uniform porosity parameters for a whole urban area entails serious limitations. First, there is no chance of reproducing the spatial

variability of the flow field within the urban zone; second, for increasingly larger built-up areas, uniform porosity parameters are as difficult to estimate as meaningless, and their use is not justified from a physical point of view.

Model application to real urban layouts, considering spatially variable porosity parameters, is still an open issue for porosity models in differential form and, in particular, for the dual-porosity formulation by Ferrari et al. (2019) and Viero (2019). Then, here we propose a method of automatically extracting, for a real complex arrangement of building and garden walls, the spatial distribution of the porosity parameters needed by the above scheme.

An algorithm has been implemented to evaluate, for each computational cell of the coarse grid, i) the storage porosity, as the fraction of the area free of buildings, ii) the minimum and maximum conveyance porosities, based on the minimum path width between buildings and obstacles, and iii) the associated directions. The proposed method is tested by simulating the flooding of a real complex urban area in Italy with the Finite Volume model by Ferrari et al. (2019). The results are compared with a reference solution in which the buildings are fully resolved using a high-resolution mesh.

2 THE DUAL POROSITY APPROACH IN DIFFERENTIAL FORM

As mentioned above, the topic of this work is the definition of a general criterion for computing the maps of the four porosity parameters required by the subgrid, dual-porosity model presented in Ferrari et al. (2019) and Viero (2019). First, for the sake of clarity, the general approach is here briefly recalled.

The isotropic storage porosity, ϕ, is defined as the fraction of the area that can be occupied by water, thus accounting for the storage reduction due to the presence of buildings. The terms Ψ_L, Ψ_T and α, which are introduced in the momentum equations in tensor form (Viero & Valipour, 2017), are porosity-related parameters accounting for the reduced conveyance, the presence of preferential flow pathways, and the alteration in the flow direction, which are typically related to alignment of buildings and obstacles.

In a 1D frame, the conveyance porosity is defined as the ratio between the width of the narrowest cross-section and the total width, i.e. the width ratio of the channel contraction (Defina & Viero 2010). In a 2D frame, it is evaluated in a similar fashion along principal directions (here assumed orthogonal for sake of simplicity) of maximum (longitudinal, L) and minimum (transverse, T) conveyance. The parameter α represents the rotation angle between the L-T frame and the model frame x-y. A sketch of the four porosity parameters (ϕ, Ψ_L, Ψ_T, α) is shown in Figure 1.

This dual-porosity model was implemented in two different 2D hydrodynamic models. Ferrari et al. (2019) included the scheme in PARFLOOD, a GPU-enhanced Finite Volume model on Cartesian and multi-resolution grids (Vacondio et al. 2014, 2017); Viero (2019) used 2DEF, a Finite Element, mixed Eulerian-Lagrangian model on staggered unstructured meshes (Viero et al. 2013, 2014, 2019). In the PARFLOOD and 2DEF models, the implementation of the dual-porosity model was slightly different; Viero (2019) used the conveyance porosity in

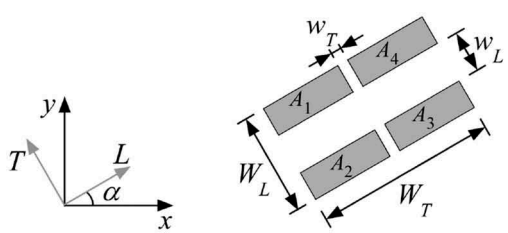

$$\phi = 1 - \frac{A_1 + A_2 + A_3 + A_4}{A_{tot}}$$

$$\psi_L = \frac{w_L}{W_L}$$

$$\psi_T = \frac{w_T}{W_T}$$

Figure 1. Definition of the four porosity parameters adopted in the dual-porosity scheme, for the sketched grid cell including four buildings and having area $A_{tot} = W_L \cdot W_T$.

tensor form to express both acceleration terms and friction losses, whereas Ferrari et al. (2019) used the conveyance porosity for friction losses and the storage porosity for accelerations. Both the schemes provided reasonably good results. In the present work, the effectiveness of the porosity parameters distribution for a real urban layout is tested using the model by Ferrari et al. (2019), which solves the following equations:

$$\begin{cases} \frac{\partial \eta}{\partial t} + \frac{\partial uh}{\partial x} + \frac{\partial vh}{\partial y} = -\frac{h}{\phi}\left(u\frac{\partial \phi}{\partial x} + v\frac{\partial \phi}{\partial y}\right) \\ \frac{\partial uh}{\partial t} + \frac{\partial}{\partial x}\left[u^2 h + \frac{1}{2}g(\eta^2 - 2\eta z)\right] + \frac{\partial uvh}{\partial y} = -g\eta\frac{\partial z}{\partial x} - \frac{uh}{\phi}\left(u\frac{\partial \phi}{\partial x} + v\frac{\partial \phi}{\partial y}\right) \\ \qquad -gh\frac{n^2 u_{eL}\sqrt{u_{eL}^2+u_{eT}^2}}{h^{4/3}}\cos\alpha + gh\frac{n^2 u_{eT}\sqrt{u_{eL}^2+u_{eT}^2}}{h^{4/3}}\sin\alpha \\ \frac{\partial vh}{\partial t} + \frac{\partial uvh}{\partial x} + \frac{\partial}{\partial y}\left[v^2 h + \frac{1}{2}g(\eta^2 - 2\eta z)\right] = -g\eta\frac{\partial z}{\partial y} - \frac{vh}{\phi}\left(u\frac{\partial \phi}{\partial x} + v\frac{\partial \phi}{\partial y}\right) \\ \qquad -gh\frac{n^2 u_{eL}\sqrt{u_{eL}^2+u_{eT}^2}}{h^{4/3}}\sin\alpha - gh\frac{n^2 u_{eT}\sqrt{u_{eL}^2+u_{eT}^2}}{h^{4/3}}\cos\alpha \end{cases} \tag{1}$$

where η is the water surface elevation, z the bottom elevation, $h = \eta - z$, g is gravity, n the Manning coefficient, u, v the velocity components in x and y directions, and u_{eL}, u_{eT} the effective flow velocities along L and T axis ($u_{eL} = \phi u_L/\Psi_L, u_{eT} = \phi u_T/\Psi_T$). It's worth noting that the well-balanced formulation in Eqs. (1) allows including the porosity-related effects (both iso- and anisotropic) by introducing additional source terms in the classical 2D-SWEs (Ferrari et al. 2019).

3 COMPUTATION OF THE POROSITY FIELDS

In previous works dealing with differential formulations of porosity models, the porosity parameters were usually evaluated at the district scale (e.g. Guinot & Soares-Frazão 2006, Soares-Frazão et al. 2008, Cea & Vázquez-Cendón 2010, Ferrari et al. 2019, Viero 2019). This means that a unique value of the storage porosity, ϕ, is computed as the ratio between the area available to the water and the total urbanized area. In this way, any information on the arrangement of buildings within the urbanized area is neglected; thus, the model can provide reasonable insights in terms of global resistance exerted by the urbanized area on the surrounding flow; within the urbanized area, only averaged information can be achieved.

In this work, the four porosity parameters (ϕ, Ψ_L, Ψ_T, α) are supposed to vary inside the built-up area, so as to account for the spatial distribution of obstacles and preferential flow paths within the urban area. This is expected to improve the description of the effects exerted by buildings on the flooding, both close and inside the urban area, at a spatial scale comparable to the (coarse) mesh resolution. Obviously, only a refined grid with resolved buildings can accurately capture small-scale flow features in urban flooding.

The same basic idea has been tested by Soares-Frazão et al. (2018) in the framework of single-porosity models (plus drag terms in tensor form), highlighting the benefits of accounting for distributed porosities based on the actual layout of buildings and streets.

3.1 *Procedure overview*

The extraction of porosity parameters from geometrical information is far more complicated for the above dual-porosity model than for the single-porosity model. While the computation of the storage porosity is straightforward (Figure 2a), the major difficulty stems from the joint estimation of conveyance principal components and the associated angle. Indeed, the conveyance porosity is directionally-dependent, and the angles that define the principal directions are not known a-priori.

To characterize the directionally-dependent conveyance porosity, the idea is to span all the possible flow directions in the range $[0, 180°[$, considering N_α discrete intervals identified by index $k \in [1, N_\alpha]$. For each hypothetical mean flow direction, at an angle α_k to the y axis

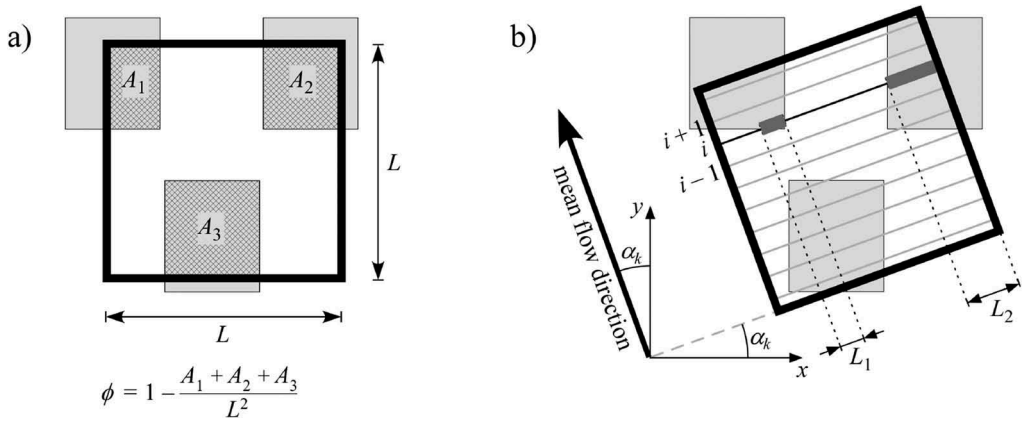

Figure 2. For a single computational cell (square with solid black line), the sketch depicts the procedure used to evaluate: a) the storage porosity, and b) the conveyance porosity for one of the mean flow directions to be tested, identified by α_k. A_1, A_2, A_3 are the building areas that overlap the computational cell.

(Figure 2b), we can define the associated conveyance porosity $\Psi(\alpha_k)$ according to the definition of Figure 1. Finally, based on the behaviour of the function $\Psi(\alpha_k)$, a proper criterion should allow identifying the principal components of the conveyance porosity (Ψ_L, Ψ_T) and the associated angle α (Figure 1). The algorithm that implements this procedure, to be applied to each computational cell, is made-up of the following steps:

1. Identify the buildings and obstacles whose footprint intersects the cell, whose size is $L \times L$;
2. Compute the storage porosity, ϕ, which is the complement to unity of the fraction of cell area occupied by buildings (Figure 2a), using any polygons intersection routine;
3. Span all the sampling directions, by changing α_k in the interval $[0, 180°[$. Given a number of directions to be considered N_α, the angular spacing (in degrees) is $\Delta\alpha = 180°/N_\alpha$. The k-th sampling direction is $\alpha_k = (k-1) \cdot \Delta\alpha$, with $k \in [1, N_\alpha]$;
4. Segment sampling. For each α_k direction, the cell is temporarily rotated by α_k and sampled with N_s equispaced segments (denoted with index i), with spacing $d_s = L/N_s$ (Figure 2b);
5. Evaluate the free length for the N_s segments. For each segment i, once detected the N_j parts overlapping the building footprints (L_1 and L_2 in Figure 2b), the total free length is computed as $L_i^{free} = L - \sum_{j=1}^{N_j} L_j$.
6. Evaluate the conveyance porosity for direction α_k as the ratio of the minimum free length to the segment length, $\Psi_{\alpha_k} = \min(L_i^{free})/L$;
7. Find the angle α for which the (reciprocally orthogonal) principal components of the conveyance porosity Ψ_L and Ψ_T are closest to the maximum and minimum values among the N_α values of Ψ_{α_k}, respectively. The goal is achieved by finding α_k such that the product $(1 - \Psi_{\alpha_k}) \cdot \Psi_{\alpha_k - 90°}$ is maximum;
8. Determine Ψ_L and Ψ_T. Since minimum and maximum values of Ψ_{α_k} are not always orthogonal to each other, and considering the importance of taking Ψ_T as the minimum value of conveyance to represent blocking features correctly, we take $\Psi_L = \Psi_{\alpha - 90°}$ and $\Psi_T = \min_k \Psi_{\alpha_k}$.

It is worth noting that this procedure is carried out as a pre-processing step and the resulting parameters are assumed constant during the simulation.

4 APPLICATION TO A REAL URBAN DISTRICT

The method described in the previous section is tested by modelling the flooding of the real urban layout shown in Figure 3, a highly urbanized district of Spinea town in Northern Italy

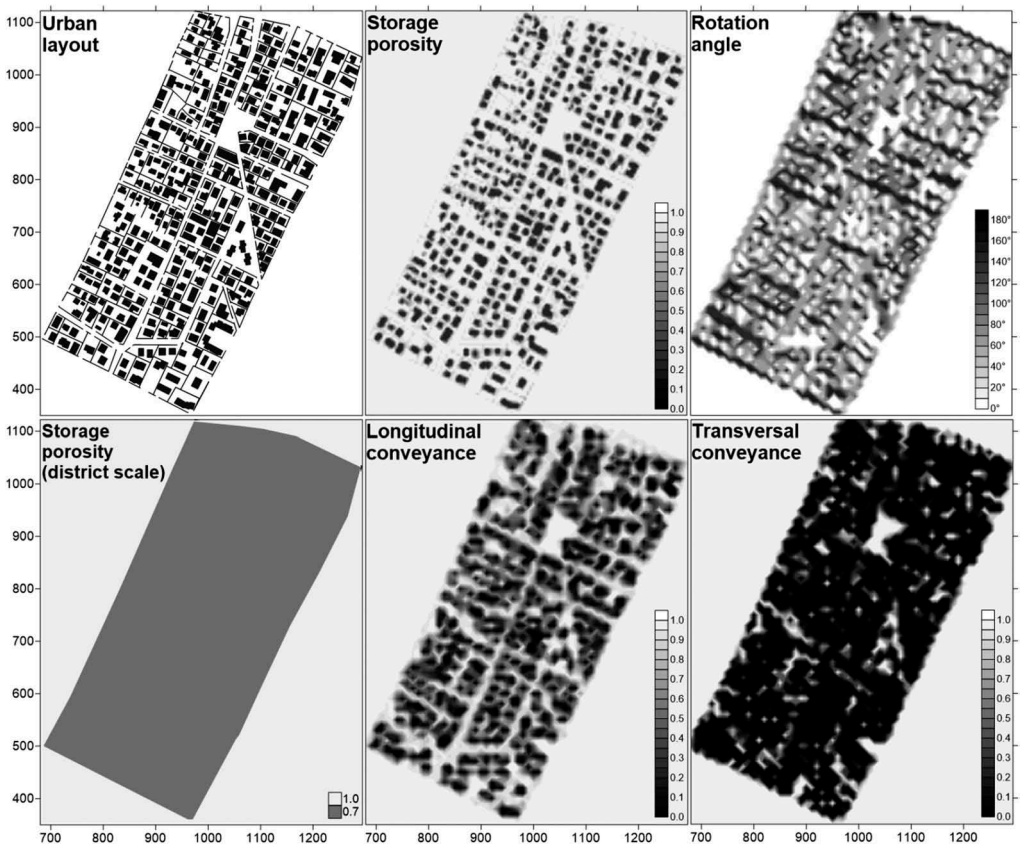

Figure 3. Porosity fields for the Spinea (Northern Italy) case study on a grid with cellsize 10 m. For comparison purposes, averaged storage porosity evaluated at the district scale is also reported.

(Viero, 2019). The domain is assumed to be characterized by a southward bottom slope of 0.09%, and a constant Manning coefficient $n = 0.03$ $\mathrm{m}^{-1/3}\mathrm{s}$. The initially dry domain is flooded from the central part of the northern edge by prescribing a 2 h long Gamma-type inflow hydrograph (Ferrari et al. 2019) with a peak value of about 600 m^3/s. Free outflow is imposed at the southern edge of the domain, whereas a free slip boundary condition is set elsewhere.

The flooding of this urban area is first modelled solving the classical 2D-SWEs on a high-resolution grid, in which the buildings are explicitly resolved according to the building hole approach (Schubert & Sanders, 2012). This solution is taken as the reference solution to test the effectiveness of the porosity fields provided by the procedure described above.

4.1 *Numerical model*

The simulations for both building hole (refined solution) and building porosity (anisotropic solution) approaches were performed with the PARFLOOD 2D finite volume model (Vacondio et al. 2014, 2016, 2017, Ferrari et al. 2018, 2020), which solves either the classical 2D-SWEs or the porous 2D-SWEs with anisotropic friction.

In its classical version, the hydrodynamic model solves the 2D-SWEs preserving the *C-property* also in presence of wet-dry fronts, regardless the slope source term discretisation (see Vacondio et al. 2014 for further details). Numerical fluxes at the cell interfaces are computed using the HLLC approximate Riemann solver (Toro 2001). A second order of accuracy both

in space and in time is achieved by reconstructing the conserved variables at the cell edges according to the linear MUSCL technique with the minmod limiter (Toro 2001), and by updating the conserved variables at each time step with the second order Runge-Kutta method. The set of partial differential equations is solved on structured grids, both Cartesian (Vacondio et al. 2014) and multi-resolution Block Uniform Quadtree (Vacondio et al. 2017). Finally, significant reduction of the run times is achieved due to the implementation in the framework of the CUDA/C++ architecture that exploits parallel computation offered by NVIDIA Graphic Processing Units (GPUs). Alternatively, PARFLOOD solves the porous 2D-SWEs with anisotropic friction (1).

All the simulations were run on a NVIDIA® Tesla® P100 GPU.

4.2 *Results*

A structured Cartesian grid with square cells is adopted to discretize the domain in all the simulations: the mesh size, Δx, is 0.5 m for the refined solution, whereas grids with Δx equal to 5, 10, 20 and 50 m are tested for the porous ones. The spatial distribution of the four porosity parameters ($\phi, \Psi_L, \Psi_T, \alpha$) are computed as described in Sect. 3. An example of the resulting parameters for Δx=10 m (evaluated with $N_\alpha = 36$, $\Delta\alpha = 5^\circ$ and $d_s = 10$ cm) is shown in Figure 3.

The water depths at the flood peak ($t \cong 0.6$ h) are shown in Figure 4 for the reference solution and for the porosity model with grid resolution of 5 m and 10 m. In order to facilitate the comparison, the building footprints have been added to the porous results, even if they were not explicitly resolved in the computation.

Figures 4 and 5 show that the porous scheme, and hence the parameter computation, allows capturing the most relevant features of the flooding, such as the deeper water depths north of the built-up area and the lower depths downstream (south-east zone), the high velocity zone at the northern edge of the urban patch, the moderate velocities at the western edge, and the low velocities at south-east. The main differences with the reference solution occur in the south part of the domain, where the porosity scheme slightly overestimates both the water depth and velocity.

A quantitative comparison is assessed by evaluating the L_2 error norm for maximum water depth and maximum velocity, within (L_{2_IN}) and outside (L_{2_OUT}) the built-up area, as:

$$L_2(v) = \sqrt{\frac{1}{N}\sum_{i=1}^{N}\left[v_{por}^i - v_{res}^i\right]^2} \tag{2}$$

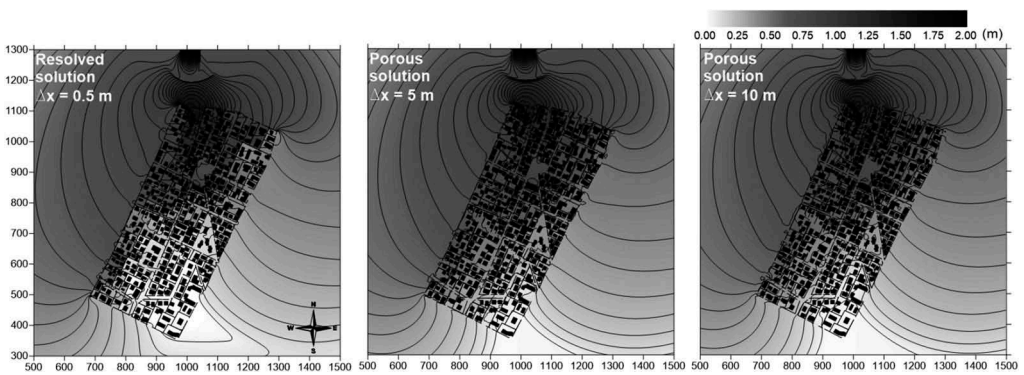

Figure 4. Water depth at the arrival of the flood peak.

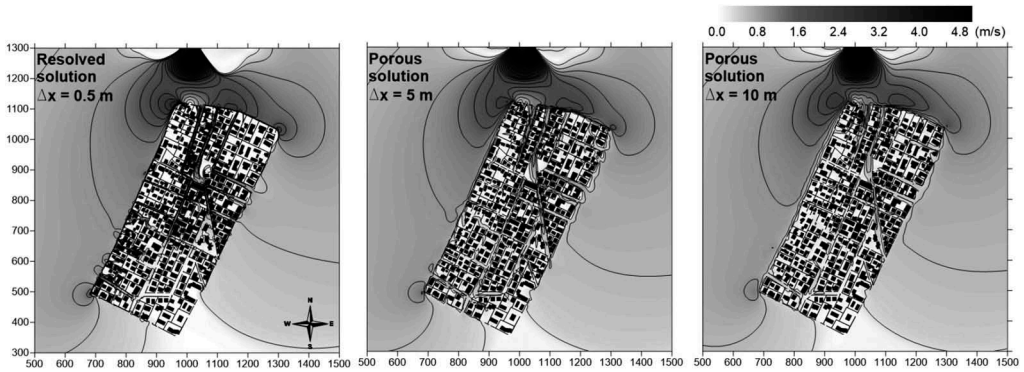

Figure 5. Velocity magnitude fields at the arrival of the flood peak.

Table 1. Simulation ID, urban modelling approach, cell size Δx, cell number N, run time t, maximum water depth (L_2^h) and velocity magnitude (L_2^u) norms within (IN) and outside (OUT) the built-up area.

ID	Building approach	Δx (m)	N (10^3)	t (min)	$L^h_{2\_IN}$ (m)	$L^u_{2\_IN}$ (ms^{-1})	$L^h_{2\_OUT}$ (m)	$L^u_{2\_OUT}$ (ms^{-1})
1	Resolved	0.5	7045.4	119.47	-	-	-	-
2	Porosity	5	70.94	0.24	0.19	0.28	0.03	0.04
3	Porosity	10	17.87	0.06	0.18	0.34	0.03	0.05
4	Porosity	20	4.54	0.03	0.22	0.38	0.04	0.10
5	Porosity	50	0.76	0.01	0.26	0.47	0.05	0.16

where N is the number of cells (free of buildings in the refined simulation) within and outside the urban area, respectively, and v the variable of interest (maximum water depth h_{max} or velocity magnitude u_{max}) resulting from the porous (v_{por}) and the reference (v_{res}) solutions.

The resulting error norm values (Table 1) do not vary significantly for $\Delta x \leq 20$ m, and become higher for $\Delta x = 50$ m, confirming that the mesh resolution has to be comparable to the characteristic building size to obtain reliable results. In this test, $\Delta x = 50$ m is two order of magnitude larger than the reference one.

For what concerns the run times, the high-resolution reference simulation takes about 2 h, whereas the porous run with $\Delta x = 5$ m only takes 14 s (Table 1). This is obviously related to the number of computational cells, which in the former case is about two order of magnitude higher than in the latter one, and to the use of larger time steps. The advantage of using porous modelling to reduce the run times, meanwhile describing the effects exerted by urban areas, is confirmed.

5 DISCUSSION

Some aspects of the proposed procedure to compute the four porosity parameters in real urban areas deserve to be further discussed.

The choice of using the minimum free length among all the sampling segments is consistent with the hypothesis assumed in Ferrari et al. (2019) and Viero (2019), i.e. that the flow in the cell is mainly governed by the narrowest passage. One may expect that in this way the resistances produced by buildings and obstacles are overestimated; quite the opposite, the model application to the Spinea case study showed that the celerity of the flood wave within the

urban area is greater in the porous case than in the reference solution, suggesting that the resistance due to buildings are underestimated.

Indeed, a careful inspection of the matter reveals that the proposed approach for estimating the porosity parameters may lead to overestimation of the actual conveyance. An example is represented by not-aligned (staggered) buildings separated by relatively narrow streets, in which the wake produced by one obstacle can partially occlude the passage between downstream buildings. This occurrence can not be detected by the "segment sampling" approach described in Sect. 3.1, as each segment does not consider anything on the upstream or downstream obstacles.

Other approaches could be attempted in the future to enhance the conveyance estimation. For instance, the cell could be sliced in (as few as thicker) strips, rather than sampled by many segments, and the actual conveyance could be accounted for by computing the (minimum) free length of the strips (Ferrari & Viero, 2020).

6 CONCLUSIONS

This work presented a procedure to compute the spatial distribution of the four porosity parameters required by the dual-porosity model recently proposed by Ferrari et al. (2019) and Viero (2019), and it represents a step forward for the modelling of floods in complex urban layout adopting porosity schemes. All the porosity parameters are computed on a cell-by-cell basis and not at the district scale: as a result, they are no more uniform in the whole urban area, as in previous works with porosity models in differential form.

The results provided by the PARFLOOD model with the porosity fields computed with the proposed procedure are promising, as confirmed by qualitative and quantitative comparison with a reference solution obtained by solving the same problem on a high-resolution grid.

Additional testing of the procedure is required to validate the proposed approach, and some directions of improvement have been suggested.

REFERENCES

Bruwier, M., Archambeau, P., Erpicum, S., Pirotton, M. & Dewals, B. 2017. Shallow-water models with anisotropic porosity and merging for flood modelling on Cartesian grids. *Journal of Hydrology* 554: 693–709.

Cea, L. & Vázquez-Cendón, M.E. 2010. Unstructured finite volume discretization of two-dimensional depth-averaged shallow water equations with porosity. *International Journal for Numerical Methods in Fluids* 63(8): 903–930.

Cozzolino, L., Pepe, V., Cimorelli, L., D'Aniello, A., Della Morte, R. & Pianese, D. 2018. The solution of the dam-break problem in the Porous Shallow water Equations. *Adv in Water Resources* 114: 83–101.

Defina, A. 2000. Two-dimensional shallow flow equations for partially dry areas. *Water Resources Research* 36: 3251.

Defina, A. & Viero, D.P. 2010. Open channel flow through a linear contraction. *Physics of Fluids* 22: 36602.

Ferrari, A., Vacondio, R., Dazzi, S. & Mignosa, P. 2017. A 1D-2D Shallow Water Equations solver for discontinuous porosity field based on a Generalized Riemann Problem. *Advances in Water Resources* 107: 233–249.

Ferrari, A., D'Oria, M., Vacondio, R., Dal Palù, A., Mignosa, P. & Tanda, M.G. 2018. Discharge hydrograph estimation at upstream-ungauged sections by coupling a Bayesian methodology and a 2-D GPU shallow water model. *Hydrology and Earth System Sciences* 22(10): 5299–5316.

Ferrari, A., Viero, D.P., Vacondio, R., Defina, A. & Mignosa, P. 2019. Flood inundation modeling in urbanized areas: A mesh-independent porosity approach with anisotropic friction. *Advances in Water Resources* 125: 98–113.

Ferrari, A., Dazzi, S., Vacondio, R. & Mignosa, P. 2020. Enhancing the resilience to flooding induced by levee breaches in lowland areas: a methodology based on numerical modelling. *Natural Hazards Earth System Sciences* 20: 59–72.

Ferrari, A. & Viero, D.P. 2020. Floodwater pathways in urban areas: computing porosity fields for anisotropic subgrid models in differential form. *Journal of Hydrology*, submitted.
Finaud-Guyot, P., Delenne, C., Lhomme, J., Guinot, V. & Llovel, C. 2010. An approximate-state Riemann solver for the two-dimensional shallow water equations with porosity. *International Journal for Numerical Methods in Fluids* 62(12): 1299–1331.
Guinot, V. 2012. Multiple porosity shallow water models for macroscopic modelling of urban floods. *Advances in Water Resources* 37: 40–72.
Guinot, V., & Soares-Frazão, S. 2006. Flux and source term discretization in two-dimensional shallow water models with porosity on unstructured grids. *Int Journal Numerical Methods in Fluids* 50(3): 309–345.
Guinot, V., Sanders, B.F. & Schubert, J.E. 2017. Dual integral porosity shallow water model for urban flood modelling. *Advances in Water Resources* 103: 16–31.
Özgen, I., Liang, D. & Hinkelmann, R. 2016. Shallow water equations with depth-dependent anisotropic porosity for subgrid-scale topography. *Applied Mathematical Modelling* 40(17-18): 7447–7473.
Sanders, B.F., Schubert, J.E. & Gallegos, H.A. 2008. Integral formulation of shallow-water equations with anisotropic porosity for urban flood modeling. *Journal of Hydrology* 362(1-2): 19–38.
Schubert, J.E. & Sanders, B.F. 2012. Building treatments for urban flood inundation models and implications for predictive skill and modeling efficiency. *Advances in Water Resources* 41: 49–64.
Soares-Frazão, S., Lhomme, J., Guinot, V. & Zech, Y. 2008. Two-dimensional shallow-water model with porosity for urban flood modelling. *Journal of Hydraulic Research* 46(1): 45–64.
Soares-Frazão, S., Franzini, F., Linkens, J. & Snaps, J.-C. 2018. Investigation of distributed-porosity fields for urban flood modelling using single-porosity models. *E3S Web of Conferences* 40: 06040.
Toro, E.F. 2001. *Shock Capturing Methods for Free Surface Shallow Water Flows*. John Wiley.
Vacondio, R., Dal Palù, A. & Mignosa, P. 2014. GPU-enhanced Finite Volume Shallow Water solver for fast flood simulations. *Environmental Modelling & Software* 57: 60–75.
Vacondio, R., Aureli, F., Ferrari, A., Mignosa, P. & Dal Palù, A. 2016. Simulation of the January 2014 flood on the Secchia River using a fast and high-resolution 2D parallel shallow-water numerical scheme. *Natural Hazards* 80(1): 103–125.
Vacondio, R., Dal Palù, A., Ferrari, A., Mignosa, P., Aureli, F. & Dazzi, S. 2017. A non-uniform efficient grid type for GPU-parallel Shallow Water Equations models. *Environmental Modelling & Software* 88: 119–137.
Varra, G., Pepe, V., Cimorelli, L., Della Morte, R. & Cozzolino, L. 2019. On the integral and differential porosity models for urban flooding simulation. *Advances in Water Resources* 136: 103455.
Velickovic, M., Zech, Y. & Soares-Frazão, S. 2017. Steady-flow experiments in urban areas and anisotropic porosity model. *Journal of Hydraulic Research* 55(1): 85–100.
Viero, D.P., D'Alpaos, A., Carniello, L. & Defina, A. 2013. Mathematical modeling of flooding due to river bank failure. *Advances in Water Resources* 59: 82–94.
Viero, D.P., Peruzzo, P., Carniello, L. & Defina, A. 2014. Integrated mathematical modeling of hydrological and hydrodynamic response to rainfall events in rural lowland catchments. *Water Resources Research* 50: 5941–5957.
Viero, D.P. & Valipour, M. 2017. Modeling anisotropy in free-surface overland and shallow inundation flows. *Advances in Water Resources* 104: 1–14.
Viero, D.P., Roder, G., Matticchio, B., Defina, A. & Tarolli, P. 2019. Floods, landscape modifications and population dynamics in anthropogenic coastal lowlands: The Polesine (northern Italy) case study. *Science of the Total Environment* 651: 1435–1450.
Viero, D.P. 2019. Modelling urban floods using a finite element staggered scheme with an anisotropic dual porosity model. *Journal of Hydrology* 568: 247–259.